JACS
JOURNAL OF THE AMERICAN CHEMICAL SOCIETY

Article

pubs.acs.org/JACS

Activity Descriptor Identification for Oxygen Reduction on Nonprecious Electrocatalysts: Linking Surface Science to Coordination Chemistry

Nagappan Ramaswamy, Urszula Tylus, Qingying Jia, and Sanjeev Mukerjee*

Northeastern University Center for Renewable Energy Technology, Department of Chemistry and Chemical Biology, Northeastern University, 317 Egan Research Center, 360 Huntington Avenue, Boston, Massachusetts 02115, United States

Supporting Information

ABSTRACT: Developing nonprecious group metal based electrocatalysts for oxygen reduction is crucial for the commercial success of environmentally friendly energy conversion devices such as fuel cells and metal−air batteries. Despite recent progress, elegant bottom-up synthesis of nonprecious electrocatalysts (typically Fe−N_x/C) is unavailable due to lack of fundamental understanding of molecular governing factors. Here, we elucidate the mechanistic origin of oxygen reduction on pyrolyzed nonprecious catalysts and identify an activity descriptor based on principles of surface science and coordination chemistry. A linear relationship, depicting the ascending portion of a volcano curve, is established between oxygen-reduction turnover number and the Lewis basicity of graphitic carbon support (accessed via C 1s photoemission spectroscopy). Tuning electron donating/withdrawing capability of the carbon basal plane, conferred upon it by the delocalized π-electrons, (i) causes a downshift of e_g-orbitals (d_{z^2}) thereby anodically shifting the metal ion's redox potential and (ii) optimizes the bond strength between the metal ion and adsorbed reaction intermediates thereby maximizing oxygen-reduction activity.

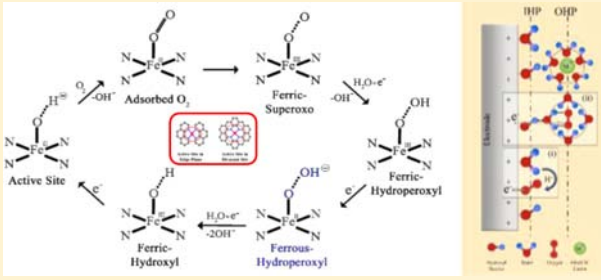

INTRODUCTION

Parallel forces aiming to achieve climate stabilization and energy independence have accelerated the pursuit of clean and efficient electrochemical energy conversion devices such as fuel cells and metal−air batteries.[1,2] These devices are expected to play definitive roles in the widespread utilization of renewable energy sources.[3] At the crux of these devices lies the grand challenge of developing highly active, inexpensive, and stable electrocatalysts for the kinetically sluggish oxygen reduction reaction (ORR).[4−6] In accordance to Sabatier's principle of catalysis, designing bottom-up approaches for catalyst synthesis involves identification and optimization of various material properties that govern reaction rates on active surfaces.[7] For instance, d-band vacancy/center,[8,9] surface lattice strain[10] (in platinum-based systems), and e_g-orbital filling of transition metals[11] (in perovskite-based systems) have been identified as fundamental material properties that act as ORR activity descriptors. In essence, to maximize surface catalytic activity, tuning such electronic and structural material properties optimizes the d-orbital occupancy near the Fermi level; thereby achieving a fine balance between the chemisorption energy of ORR intermediates and the number of surface sites available for initial O_2 adsorption.[4,12]

The drive to replace expensive precious-metal-group (PGM) systems for ORR has led to a class of catalysts comprising transition metal ions stabilized by nitrogen functional groups on carbonaceous surfaces (Fe−N_x/C).[13−16] These active sites are adventitiously synthesized via pyrolysis of precursors containing transition metals, nitrogen, and carbon, all of them present in either the same source or different sources.[17] Potential multiplicity of active sites for initial O_2 adsorption and the lack of suitable analytical techniques complicates a lucid understanding of the nature of active sites and the reaction mechanisms in these composite catalysts.[14] Despite high activity and durability of pyrolyzed Fe−N_x/C catalysts shown recently,[18−20] current progress primarily involves an experiential approach of trial-and-error combination of precursors and pyrolysis conditions to maximize performance. Lack of fundamental understanding of the mechanistic origin of ORR and the underlying surface material properties that govern catalytic activity clearly limits further progress. Here, for the first time we present a direct structure−activity relationship between the intrinsic ORR turnover number (i.e., kinetic current-density normalized by electrochemically active site-density quantified via square-wave voltammetry) and a surface material property of pyrolyzed Fe−N_x/C catalyst, thus providing deep insight into the fundamental mechanistic origin of ORR and potentially opening the door to elegant bottom-up catalyst synthesis strategies.

Electrocatalysis on *nonpyrolyzed* metal macrocycles is governed by the nature of the (i) central metal ion and (ii) the surrounding macrocyclic ligand.[21] While d-electron density on the metal ion determines the progress of ORR via adsorbed

Received: May 31, 2013
Published: September 13, 2013

dx.doi.org/10.1021/ja405149m | J. Am. Chem. Soc. 2013, 135, 15443−15449

intermediates, the role of π-conjugated ligand is to modify the metal ion's electronic structure by relocating its redox potential.[21,22] Based on molecular-orbital approach, the end-on M−O_2 interaction primarily involves σ-type bonding between O_2 molecular orbitals and the e_g-orbital (d_{z^2}) of the transition metal ion.[21,23−25] Further in accordance to the redox mechanism,[26,27] ORR onset potential is closely linked to the metal ion's redox potential, which in turn essentially represents the e_g-orbital (d_{z^2}) energy level.[28] Thus, a downshift in energy level of e_g-orbitals away from the Fermi level anodically shifts the metal ion's redox potential leading to higher ORR onset potentials and optimizes the adsorption strength of ORR intermediates leading to higher turnover numbers. Downshift of e_g-orbitals is possible via (i) substitution of electron-withdrawing groups on the macrocycle ring[29,30] and (ii) formation of electron donor−acceptor pair between metal−macrocycle and carbon basal plane via π−π interaction (due to electron-withdrawing nature of delocalized π-electrons in carbon basal plane relative to π-electron rich macrocycle).[31] However, both these routes involve long-range noncovalent interactive forces leading to a minor potential shift (~200 mV), insufficient to cause significant change in ORR onset potential.

Here, we show that the pyrolysis step covalently integrates the Fe−N_x active site into the π-conjugated carbon basal plane, causing a dramatic anodic shift of ~600−900 mV in the metal ion's redox potential. Since the carbon basal plane constitutes an integral part of the active site rather than merely an electrically conducting high surface area support, the surface chemistry of underlying carbon needs due consideration.[32−34] We show that the electron-donating/withdrawing capability of the carbon support, conferred upon it by the delocalized π-electrons, acts as a primary activity descriptor that governs ORR electrocatalysis on pyrolyzed Fe−N_x/C active sites. In addition, we also elucidate the aspect of outer-sphere electron transfer mechanism during ORR in alkaline media, particularly in light of recent evidence highlighting the necessity to promote an inner-sphere electron transfer mechanism via direct chemisorption of desolvated O_2 on the active site.[35−37] Using iron(III) meso-tetraphenylporphine chloride (FeTPPCl) as a model system, we elucidate inner- vs outer-sphere ORR mechanisms and active-site structure evolution and, most importantly, establish scientifically relevant electrocatalytic activity trends to provide a fundamental molecular level understanding of ORR on pyrolyzed Fe−N_x/C catalysts.

RESULTS AND DISCUSSION

ORR Activity and Electron Transfer Mechanisms. Our current state of understanding of ORR mechanisms is summarized in Figure 1a.[36] In alkaline media, taking platinum surface as a starting point of illustration, ORR is understood to involve both inner- and outer-sphere electron transfer mechanisms. The well-known electrocatalytic inner-sphere electron transfer (ISET) mechanism (Figure 1a, inset i) involves chemisorption of desolvated O_2 on an oxide-free Pt-site leading to a direct/series 4e^- ORR pathway without desorption of reaction intermediates.[23,36] New evidence shows the coexistence of an outer-sphere electron transfer (OSET) mechanism (Figure 1a, inset ii), wherein the noncovalent hydrogen bonding forces between specifically adsorbed hydroxyl species (OH_{ads} acting as an outer-sphere bridge) and solvated O_2 (localized in outer-Helmholtz plane) promote a 2e^- reduction pathway forming HO_2^- anion[36] (Supplementary Figure S1, Supporting Information). As shown in Figure

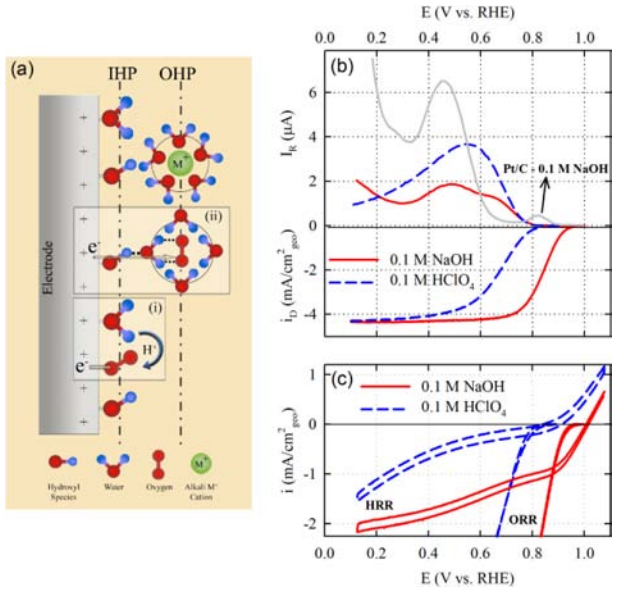

Figure 1. ORR activity and mechanisms. (a) Schematic illustration of inner-sphere (inset i) and outer-sphere (inset ii) electron transfer mechanisms during ORR in alkaline media. (IHP, inner Helmholtz plane; OHP, outer Helmholtz plane). Comparison of the electrochemical characteristics of an Fe−N_x/C catalyst (pyrolyzed at 800 °C) in O_2-saturated 0.1 M $HClO_4$ and 0.1 M NaOH electrolytes showing (b) ORR activity (i_D) and concomitant ring current (I_R) due to hydrogen peroxide oxidation. Also shown for comparison in panel b is the ring-current profile measured during ORR on a Pt/C catalyst deposited on the disk electrode. (c) Hydrogen peroxide reduction reaction (HRR) activity in argon-saturated electrolytes containing 3.5 mM H_2O_2 in comparison to ORR. HRR experiments were carried out by scanning the potential in the cathodic direction starting from the open-circuit potential so that any influence due to O_2 evolved from H_2O_2 electro-oxidation is avoided. Scan rate, 20 mV/s; rotation rate, 900 rpm; E_{ring} = 1.1 V vs RHE in 0.1 M NaOH and 1.3 V vs RHE in 0.1 M $HClO_4$; Fe−N_x/C loading, 100 μg/cm^2; Pt/C loading, 15 μg_{Pt}/cm^2 on 5.61 mm glassy carbon disk at 900 rpm.

1b, a HO_2^- anion intermediate generated via the OSET mechanism on Pt−OH_{ads} sites is characterized by its oxidation peak signature in ring current at ~0.8 V in alkaline media (see Supplementary Figure S1, Supporting Information; ring-current peak at ~0.45 V in alkaline media is due to carbon support). As is well-known, in acidic media OH_{ads} species from water activation primarily serve only to block O_2 chemisorption.[38,39] However, in alkaline media the OH_{ads} species not only blocks O_2 adsorption but also promotes the outer-sphere process to yield a stable peroxide intermediate. As elucidated by Bard,[35] this necessitates the promotion of an electrocatalytic inner-sphere reaction mechanism for a complete 4e^- ORR process in alkaline electrolytes. This can be achieved via facilitation of direct adsorption of desolvated O_2 on OH_{ads}-free active sites and avoiding the precipitous outer-sphere reaction of solvated O_2 with OH_{ads} covered active sites.

In alkaline media, ORR on Fe−N_x/C catalyst pyrolyzed at 800 °C (Figure 1b) commences at 0.95 V, and the concomitant peroxide-intermediate oxidation at the ring electrode does not begin until 0.8 V. More importantly, in comparison to Pt/C in 0.1 M NaOH, the characteristic ring-electrode signature at ~0.8 V for peroxide-intermediate formation via the outer-sphere process is clearly absent on the Fe−N_x/C based catalyst (only a weak shoulder in ring current at more negative potentials of 0.60 to 0.70 V is observed indicating that the OSET mechanism

dx.doi.org/10.1021/ja405149m | J. Am. Chem. Soc. 2013, 135, 15443−15449

is significantly muted). This indicates the facilitation of direct adsorption of desolvated O_2 on the active site. Further, hydrogen peroxide reduction reaction (HRR) in 0.1 M NaOH (Figure 1c) is kinetically favored on Fe−N_x/C active sites such that any peroxide intermediate formed during ORR in 0.1 M NaOH will be immediately reduced to the $4e^-$ product. Contrarily, in 0.1 M $HClO_4$ (Figure 1b), the onset potential for both ORR on the disk electrode and concomitant peroxide-intermediate oxidation on the ring electrode is at 0.8 V, indicating the immediate formation of stable peroxide intermediate upon commencement of ORR. In corroboration to this, HRR activity on Fe−N_x/C in acidic media (Figure 1c) is kinetically unfavorable due to weak binding or destabilization of hydrogen peroxide such that the H_2O_2 intermediate formed during ORR is desorbed into the bulk electrolyte (unless at very low potentials of E < 0.5 V where HRR activity in 0.1 M $HClO_4$ is evidenced concomitant to decrease in ring current). Most importantly, the 3−4 orders of magnitude higher ORR activity on Fe−N_x/C in alkaline media (i.e., $E_{1/2}$ = 837 ± 8 mV in 0.1 M NaOH against $E_{1/2}$ = 667 ± 12 mV in 0.1 M $HClO_4$; Supplementary Table S1, Figure S2, Supporting Information) is due to the apparent electrocatalytic activity toward the reduction of hydrogen peroxide intermediate; the lack of which in acidic media leads to higher overpotentials.

Active-Site Structure Identification. Identification of the nature of the Fe−N_x/C active site and the adsorbate site specificity were carried out using the delta-mu ($\Delta\mu$) technique, which is a surface sensitive spectral subtraction methodology in the X-ray absorption near-edge spectra (XANES) region[40,41] (see Supplementary Methods, Supporting Information). For a carbon supported iron−porphyrin complex subjected only to a mild pyrolysis at 300 °C, the Fe K-edge XANES (Figure 2a) is essentially reminiscent of the original porphyrin macrocycle[42] (Supplementary Figure S3, Supporting Information). Subtraction of Fe K-edge XANES region taken at two different potentials of 0.1 and 0.9 V in 0.1 M NaOH yields the experimental $\Delta\mu$ spectrum (Figure 2a), in which the positive-peak feature (boxed region) indicates the absorption probability difference at the pre-edge energy. This feature is safely assigned as a signature for the existence of the metal center in a square-planar, centrosymmetric Fe^{2+}−N_4 environment at 0.1 V (forbidden XANES pre-edge) undergoing redox transition to a pentacoordinate (H)O−Fe^{3+}−N_4 environment at 0.90 V (allowed pre-edge). The structural model (Figure 2a, inset) utilized in the simulation of theoretical $\Delta\mu$ spectra (via FEFF8.0 code,[43] see Supplementary Methods, Supporting Information) essentially represents the FeN_4C_{12} cluster inscribed in the original iron−porphyrin macrocycle cavity (Figure 2b). After 300 °C pyrolysis, the coordination environment of the original precursor porphyrin macrocycle is clearly retained with all the carbon methine bridges intact indicating no major destruction of the macrocycle.[44] Contrarily, Fe K-edge XANES spectra of Fe−N_x/C catalyst pyrolyzed at 800 °C (Figure 2c) is predominantly characteristic of metallic iron that precludes proper analysis of the active site (Supplementary Figure S3, Supporting Information). However, careful analysis of the corresponding experimental $\Delta\mu$ spectrum clearly indicates the positive-peak feature at the pre-edge energy signifying that the metal-center Fe^{2+} is in a centrosymmetric environment and undergoes the redox transition to Fe^{3+}. Figure 2c also shows the theoretical $\Delta\mu$ spectrum that mimics the line shape of the experimental $\Delta\mu$ for the 800 °C pyrolyzed catalyst (Supplementary Figure S4, Supporting Information, shows

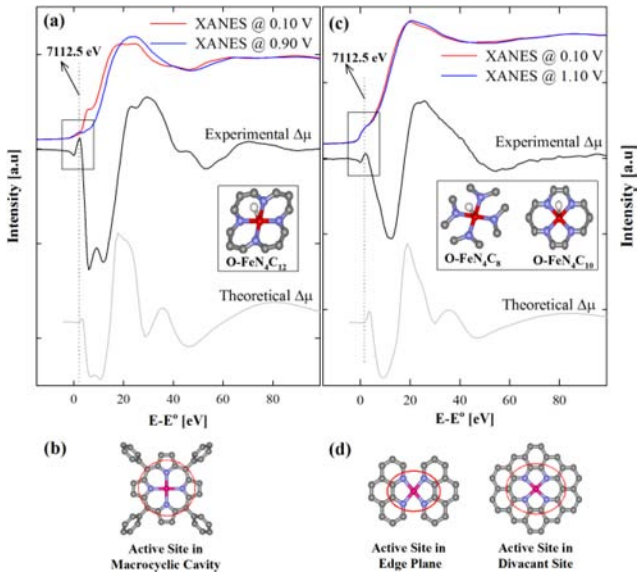

Figure 2. Active site structure identification. Experimental XANES and $\Delta\mu$ signatures of Fe−N_x/C catalyst pyrolyzed at (a) 300 and (c) 800 °C. The $\Delta\mu$ signatures were obtained by subtracting the XANES signatures according to $\Delta\mu$ = μ(0.90 (or) 1.10 V) − μ(0.10 V). Experiments were conducted at Fe K-edge under *in situ* conditions in argon saturated 0.1 M NaOH electrolyte. Vertical dotted line indicates the pre-edge position at 7112.5 eV. Structural models shown in the insets of panels a and c were utilized for $\Delta\mu$ analysis using FEFF8 simulation. Also shown are the complete structural models of active site structures before (b) and after (d) pyrolysis at 800 °C. Color codes in structural models: red, iron; blue, nitrogen; gray, carbon; white, oxygen.

some of the unsuccessful theoretical $\Delta\mu$ fits). The molecular clusters used to simulate the theoretical $\Delta\mu$ spectrum (Figure 2c, inset) consisted of FeN_4C_z sites with either a partial (z = 10) or a complete destruction (z = 8) of the carbon methine bridges. Based on a combination of Fe K-edge XANES experiment and theoretical $\Delta\mu$ modeling, it is observed that the metal−nitrogen structural motif FeN_4C_z constitutes the active site. The immediate coordination environment of the metal active site after 800 °C pyrolysis (Figure 2d) is reminiscent of the covalent incorporation of FeN_4C_{10} active sites in crystallographic atomic defects such as the divacancy on the carbon basal plane (partially destroyed carbon methine bridges) or of FeN_4C_8 active sites in armchair edges of graphitic surfaces (complete removal of carbon methine bridges).

ORR Activity Descriptor Identification. To establish a relationship between the nature of the Fe−N_4/C active site and the fundamental molecular-level mechanistic origin of ORR activity, we begin by investigating square-wave voltammetry (SWV) profiles of FeTPPCl supported on black pearl carbon. For the nonpyrolyzed macrocycle, Figure 3a shows that (in combination with the above $\Delta\mu$ studies and *in situ* XANES results (see Supporting Figure S5, Supporting Information)) the $Fe^{2+/3+}$ redox-couple localized at 0.31 V in 0.1 M NaOH electrolyte[45] undergoes a significant anodic shift to ∼1.25 V after pyrolysis at 800 °C. Contrarily, in 0.1 M $HClO_4$ the anodic shift $Fe^{2+/3+}$ redox potential upon pyrolysis is only ∼600 mV due to proton-coupled electron transfer effect in coordination complexes as explained in Supporting Figure S6, Supporting Information. The $Fe^{2+/3+}$ peak potential in 0.1 M NaOH and full-width at half maxima (fwhm) of carbon-1s photoemission spectra of Fe−N_4/C catalysts (see Supplemen-

dx.doi.org/10.1021/ja405149m | J. Am. Chem. Soc. 2013, 135, 15443−15449

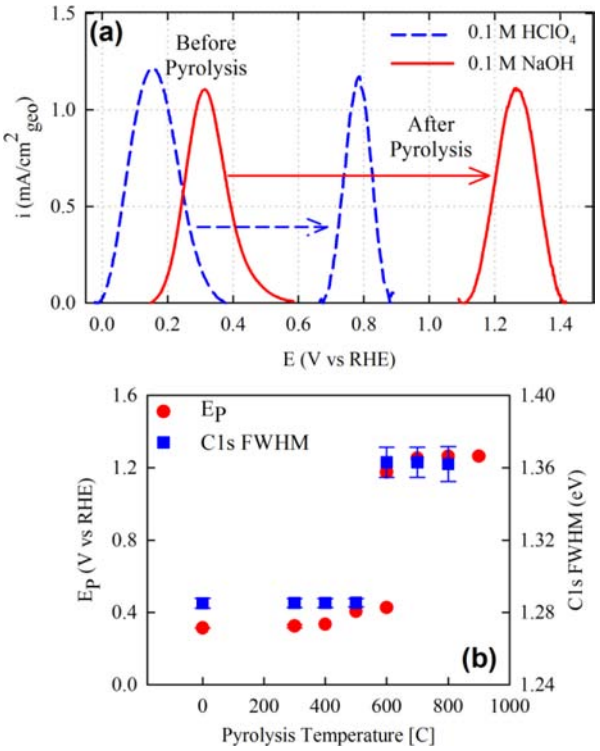

Figure 3. Redox potential of active site. (a) Square-wave voltammetry (SWV) profiles of Fe−N_x catalyst supported on black pearl carbon before and after pyrolysis at 800 °C in 0.1 M $HClO_4$ and 0.1 M NaOH electrolytes. (b) Plot showing the effect of pyrolysis temperature on Fe−N_x/C redox peak potential (E_p) in 0.1 M NaOH and full-width at half-maxima of C 1s photoemission spectra. SWV profiles after pyrolysis have been multiplied by a factor of 7 for visual comparison.

tary Methods, Supporting Information) are plotted as a function of pyrolysis temperature in Figure 3b. The C 1s spectra of sp^2-hybridized graphitic carbon is typically dominated by the asymmetric graphite peak at 284.3 eV involving transitions to the conduction π-band (1s → π^*).[46,47] While the peak position indicates the chemical environment of carbon, the fwhm is a measure of disorder in carbon structure crystallinity.[48,49] The 2p-electron overlap in the carbon basal plane yields the delocalized π-electron system that confers the chemical property of Lewis basicity to the carbonaceous supports.[32−34] Thus, C 1s fwhm is a measure of the degree of π-electron delocalization in carbon basal plane since the disorder (edge sites, defects, heteroatoms etc.) disrupts delocalization.[34,48,49] A narrow fwhm of the C 1s spectrum indicates a higher degree of delocalization and higher electron-donating capability of the carbon plane. A broader fwhm indicates a lower degree of delocalization and lower electron-donating capability (or conversely higher electron-withdrawing capability).[34] As evidenced by the sudden jump in C 1s fwhm after pyrolysis at 600 °C (Figure 3b), it is clear that the covalent integration of the Fe−N_4 active site into the carbon support causes significant perturbation of π-electron system in the carbon basal plane (Supporting Figure S7, Table S3, Supporting Information). The mechanistic origin of increased ORR activity upon pyrolysis arises from the abrupt change in ligand environment of the Fe−N_4 active site from a π-electron-rich macrocycle ring to a relatively π-electron-deficient graphitic ligand (i.e., electron-withdrawing); this electron-withdrawing nature of the graphite ligand environment causes an abrupt anodic shift in the redox potential of the metal ion and hence a higher ORR onset potential.

To further substantiate the influence of a delocalized π-electron system in the carbon basal plane, ORR activity of Fe−N_4/C catalyst pyrolyzed on various carbon supports was investigated in 0.1 M NaOH (Figure 4a). Given the similar

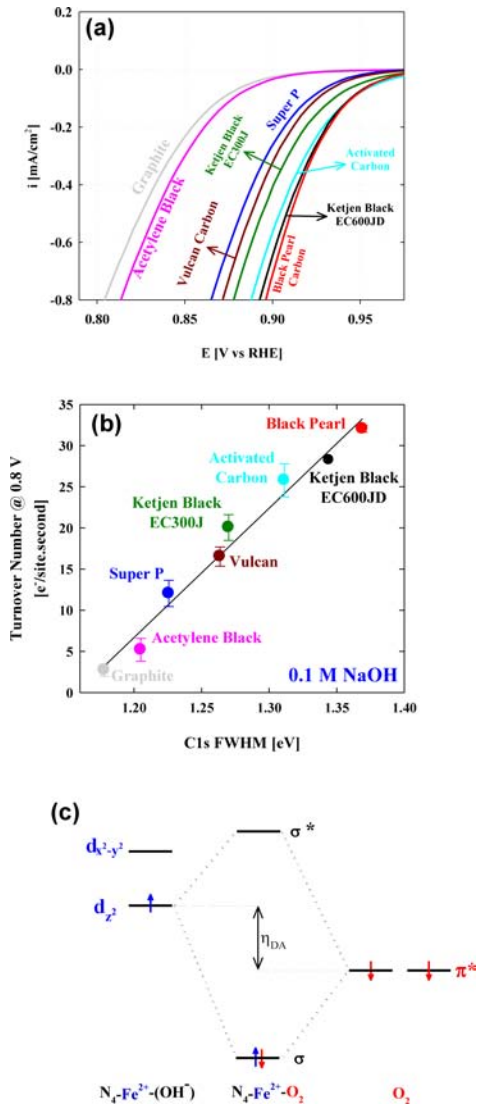

Figure 4. Relationship between ORR turnover number and electron-withdrawing character of carbon basal plane. (a) ORR activity of Fe−N_x/C catalyst (pyrolyzed at 800 °C) on various carbon supports in O_2-saturated 0.1 M NaOH electrolyte at 900 rpm rotation rate and 20 mV s^{-1} scan rate. (b) Linear relationship between ORR turnover numbers in 0.1 M NaOH electrolyte versus full-width at half-maximum of C 1s photoemission spectra. (c) Schematic illustration of intermolecular hardness (η_{DA}) parameter in Fe^{2+}−O_2 or alternatively Fe^{3+}−(O_2^-) adducts.

Tafel slopes irrespective of the nature of carbon support (Supplementary Figure S8, Supporting Information), the turnover number at 0.8 V is utilized as a measure of intrinsic ORR activity. Catalytic turnover numbers were obtained by normalizing ORR kinetic currents by electrochemically active Fe−N_4/C site-density (quantified via SWV experiments, Supplementary Figures S9 and S10 and Table S4, Supporting Information). A linear relationship (Figure 4b), depicting the

dx.doi.org/10.1021/ja405149m | J. Am. Chem. Soc. 2013, 135, 15443−15449

ascending portion of a volcano curve, is clearly observed between the ORR turnover number in 0.1 M NaOH and fwhm of C 1s photoemission spectra (Supporting Figure S11, Supporting Information, shows similar behavior in acid electrolyte). This linear dependence has two major implications for ORR: (i) the relative positioning of the e_g-orbital (d_{z^2}) of transition metal ion versus the Fermi level and (ii) intermolecular hardness parameter (η_{DA}) defined as the energy gap between the metal ion's e_g-orbital (d_{z^2}) and molecular oxygen (Figure 4c).[21,50,51] Since the Fe−N_4 active site is covalently integrated into the carbon basal plane, the electron-donating or -withdrawing nature of the carbon support arising from its delocalized π-electron system modulates the chemisorption bond strength of O_2 and reaction intermediates with the metal center (i.e., its d_{z^2} metal orbital). Relatively well-ordered carbon supports such as graphite, acetylene black, and super-P surfaces yield lower turnover numbers of 2.7 ± 0.5, 5.2 ± 1.0, and 12.0 ± 1.1 e^-/(site·s), respectively, since their electron-donating character endows higher electron density at the metal ion center. This leads to higher intermolecular hardness and causes too strong bond strength between the metal ion and ORR intermediates leading to lower ORR turnover numbers. Contrarily, highly disordered carbon supports such as activated carbon, ketjen EC600JD, and black pearl yield progressively higher turnover numbers of 25.8 ± 1.4, 28.2 ± 1.2, and 32.1 ± 0.3 e^-/(site·s), respectively, since their electron-withdrawing character causes lower electron density at the metal center and thus a downshift of the e_g-orbital (d_{z^2}) (i.e., a relatively softer Fe−O_2 adduct). This optimizes the bond strength between the metal center and the ORR intermediates and hence produces higher turnover numbers.

ORR Reaction pathway. Based on the above experimental results, the 4e^- electrocatalytic inner-sphere electron transfer mechanism in dilute alkaline media is shown in Figure 5,

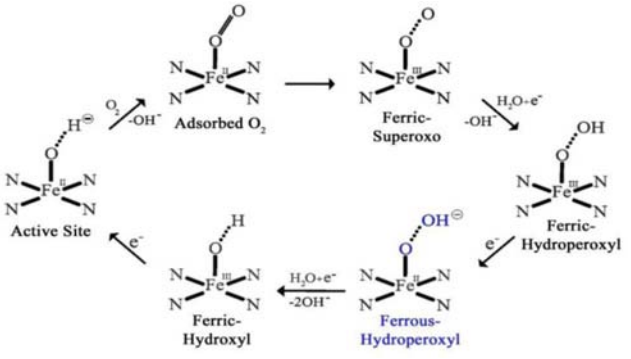

Figure 5. Proposed ORR mechanism. Catalyst cycle showing the redox mechanism involved in ORR on pyrolyzed Fe−N_x/C active sites in dilute alkaline medium.

wherein O_2 displaces the OH^- species and chemisorbs directly on the Fe^{2+} active site. The lability of the axial OH^- anion is due to the redox mechanism of ORR that ensures the reduction of pentacoordinated (H)O−Fe^{3+}−N_4 to the square-planar Fe^{2+}−N_4 active site where axial ligation is available for direct O_2 chemisorption. This ensures that the precipitous OSET mechanism is avoided on biomimetic Fe−N_4/C active sites leading to direct chemisorption of O_2 on the metal center via an inner-sphere mechanism. Once molecular O_2 adsorbs on the Fe^{2+} active site, the reaction proceeds to the ferrous−hydroperoxyl adduct via the superoxo and the ferric−hydroperoxyl states. The ferrous−hydroperoxyl adduct is very critical since its stability determines the product distribution and ORR electrocatalytic activity. For pH > 12, the Lewis basic nature of the anionic hydrogen peroxide intermediate (HO_2^-, $pK_a \approx 11.6$) leads to its apparent stabilization on Lewis acidic Fe^{2+} active sites via the formation of stabilized Lewis acid−base adduct.[52] This ensures that the catalytic cycle in alkaline media undergoes complete 4e^- transfer (Figure 5) to regenerate the active site via the formation of ferric-hydroxyl species (Supplementary Figures S12 and S13, Supporting Information, show the lack of influence of metallic iron/iron oxide impurity nanoparticles in ORR). However, in acidic media the analogous ferrous−hydroperoxyl adduct is Fe^{II}−(OHOH), wherein the protonated nature of the hydrogen peroxide intermediate (H_2O_2) negates its Lewis basic character and leads to its apparent destabilization on Fe^{2+}−N_4/C active site. This leads to higher overpotential for ORR in acidic media necessitating secondary sites to further reduce or disproportionate H_2O_2.

■ CONCLUSIONS

In this work, we have developed scientifically relevant fundamental molecular-level understanding of ORR on pyrolyzed Fe−N_4/C catalysts. The Lewis basic nature of the carbon basal plane facilitates the formation Fe−N_4 active sites on carbonaceous surfaces via the nitrogen coordinating atoms. The pyrolysis step adventititously relocates the Fe−N_4 active site from a π-electron-rich macrocyclic ligand environment to a relatively π-electron-deficient graphitic carbon environment. Divacant defective pockets and the edge-plane sites appear to provide such a π-electron-deficient environment in the carbon support; this causes a significant modification in the electron density and energy level of the e_g-orbital (d_{z^2}) of the transition metal ion leading to a significant anodic shift in its redox potential. Further, the degree of π-electron delocalization on disordered graphitic carbon basal planes can be used as a parameter to modulate the adsorption strength of ORR intermediates and the intermolecular hardness of the adducts. On biomimetic active sites, the operation of the redox mechanism ensures direct O_2 adsorption on the Fe^{2+}−N_4 active site and prevents the outer-sphere reaction of solvated O_2 with the OH_{ad}-covered active site. A unified picture is developed here by combining the principles of surface science and coordination chemistry, wherein the concepts of Sabatier's principle and intermolecular hardness are utilized to comprehensively expound the fundamental molecular level understanding of ORR on Fe−N_4/C catalysts. A unique feature of the class of pyrolyzed catalyst is the ability to tune the catalytic activity by experimentally controlling the degree of π-electron delocalization of the carbonaceous surfaces. This phenomenon will likely open the door to the development of more active and stable electrocatalysts based on biomimetic active sites on novel π surfaces.

■ METHODS

Catalyst Preparation and Physicochemical and Electrochemical Characterizations. Iron(III) meso-tetraphenylporphine chloride (FeTPPCl) was procured from Alfa Aesar. FeTPPCl was mixed with carbon in the mass ratio 1:4 and ball milled for 2 h at 400 rpm followed by pyrolysis at temperatures ranging from 300 to 1100 °C for 2 h under argon atmosphere. The iron content of the catalyst obtained in this method after pyrolysis was quantified using energy dispersive analysis of X-rays to be 3% by weight loading on carbon. All electrochemical measurements were made at room temperature using a rotating ring−disk electrode (RRDE) setup from Pine Instruments

connected to an Autolab (Ecochemie Inc., model-PGSTAT 30) bipotentiostat. Alkaline (0.1 M NaOH) and acidic (0.1 M $HClO_4$) electrolytes were prepared using sodium hydroxide pellets (semiconductor grade, 99.99%, Sigma-Aldrich) and double-distilled 70% perchloric acid (GFS Chemicals), respectively. A 30% Pt/C catalyst from BASF-ETEK (Somerset, NJ) was used as received. Catalyst inks were prepared by ultrasonically dispersing the catalyst powder in a 1:1 (by volume) ratio of water/isopropanol solution. Typical catalyst loadings employed were 100 $\mu g/cm^2$ of non-PGM catalyst or 15 $\mu g_{Pt}/cm^2$ of Pt/C catalyst on a 5.61 mm glassy carbon disk. Reversible hydrogen electrode (RHE) generated using the same electrolyte as the bulk was used as the reference electrode. The gold ring electrode was held at 1.1 V vs RHE in alkaline electrolyte and at 1.3 V vs RHE in acidic electrolyte to detect stable peroxide intermediate. Collection efficiency of the disk−ring electrode was 37.5%. All current values are normalized to the geometric area of the glassy carbon disk unless otherwise stated. Square-wave voltammetry experiments were performed using a step potential of 5 mV, potential amplitude of 20 mV, and a scan frequency of 10 Hz. Britton−Robinson buffer solutions were used for electrochemical experiments performed at electrolyte pH ranging from 2 to 12. For these pH conditions from 2 to 12, a Ag/AgCl reference electrode prepared in saturated sodium chloride was utilized for the experiments. All potentials are referred to the RHE scale unless otherwise stated. Details on the X-ray absorption spectroscopy experimental methods and $\Delta\mu$ analytical techniques are presented in the Supporting Information.

■ ASSOCIATED CONTENT

Supporting Information

Deatils on X-ray absorption experiments, $\Delta\mu$ analytical methodologies, and supporting electrochemical analysis. This material is available free of charge via the Internet at http://pubs.acs.org.

■ AUTHOR INFORMATION

Corresponding Author

s.mukerjee@neu.edu

Notes

The authors declare no competing financial interest.

■ ACKNOWLEDGMENTS

The authors deeply appreciate financial assistance from the Army Research Office under the Single Investigator grant. The authors also gratefully acknowledge the supply of platinum electrocatalysts from BASF fuel cells (Somerset, NJ, USA). Use of the National Synchrotron Light Source (NSLS) at Brookhaven National Laboratory (BNL), Upton, NY, was supported by the U.S. Department of Energy, Office of Basic Energy Sciences. Support from NSLS beamline personnel Drs. Kaumudi Pandya (X11A), Syed Khalid (X19A), and Nebojsa Marinkovic (X18B) is gratefully acknowledged. XPS experiments were performed at the Center for Nanoscale Systems (CNS), a member of the National Nanotechnology Infrastructure Network (NNIN), which is supported by the National Science Foundation under NSF Award No. ECS-0335765. CNS is part of Harvard University.

■ REFERENCES

(1) Chu, S.; Majumdar, A. *Nature* **2012**, *488*, 294.

(2) Williams, J. H.; DeBenedictis, A.; Ghanadan, R.; Mahone, A.; Moore, J.; Morrow, W. R.; Price, S.; Torn, M. S. *Science* **2012**, *335*, 53.

(3) Wagner, F. T.; Lakshmanan, B.; Mathias, M. F. *J. Phys. Chem. Lett.* **2010**, *1*, 2204.

(4) Mukerjee, S.; Srinivasan, S. In *Handbook of Fuel Cells*; John Wiley & Sons, Ltd: Hoboken, NJ, 2010.

(5) Gasteiger, H. A.; Kocha, S. S.; Sompalli, B.; Wagner, F. T. *Appl. Catal., B* **2005**, *56*, 9.

(6) Tuaev, X.; Paraknowitsch, J. P.; Illgen, R.; Thomas, A.; Strasser, P. *Phys. Chem. Chem. Phys.* **2012**, *14*, 6444.

(7) Maillard, F.; Pronkin, S.; Savinova, E. R. In *Fuel Cell Catalysis*; John Wiley & Sons, Inc.: Hoboken, NJ, 2008; p 507.

(8) Mukerjee, S.; Srinivasan, S.; Soriaga, M. P. *J. Electrochem. Soc.* **1995**, *142*, 1409.

(9) Stamenkovic, V. R.; Mun, B. S.; Arenz, M.; Mayrhofer, K. J. J.; Lucas, C. A.; Wang, G.; Ross, P. N.; Markovic, N. M. *Nat. Mater.* **2007**, *6*, 241.

(10) Strasser, P.; Koh, S.; Anniyev, T.; Greeley, J.; More, K.; Yu, C.; Liu, Z.; Kaya, S.; Nordlund, D.; Ogasawara, H.; Toney, M. F.; Nilsson, A. *Nat. Chem.* **2010**, *2*, 454.

(11) Suntivich, J.; Gasteiger, H. A.; Yabuuchi, N.; Nakanishi, H.; Goodenough, J. B.; Shao-Horn, Y. *Nat. Chem.* **2011**, *3*, 546.

(12) Greeley, J.; Stephens, I. E. L.; Bondarenko, A. S.; Johansson, T. P.; Hansen, H. A.; Jaramillo, T. F.; Rossmeisl, J.; Chorkendorff, I.; Nørskov, J. K. *Nat. Chem.* **2009**, *1*, 552.

(13) Jaouen, F.; Proietti, E.; Lefevre, M.; Chenitz, R.; Dodelet, J.-P.; Wu, G.; Chung, H. T.; Johnston, C. M.; Zelenay, P. *Energy Environ. Sci.* **2011**, *4*, 114.

(14) Dodelet, J.-P. In *N4-Macrocyclic Metal Complexes*; Zagal, J. H., Bedioui, F., Dodelet, J.-P., Eds.; Springer: New York, 2006; p 83.

(15) Wu, G.; Johnston, C. M.; Mack, N. H.; Artyushkova, K.; Ferrandon, M.; Nelson, M.; Lezama-Pacheco, J. S.; Conradson, S. D.; More, K. L.; Myers, D. J.; Zelenay, P. *J. Mater. Chem.* **2011**, *21*, 11392.

(16) Fellinger, T.-P.; Hasché, F.; Strasser, P.; Antonietti, M. *J. Am. Chem. Soc.* **2012**, *134*, 4072.

(17) Jaouen, F.; Herranz, J.; Lefévre, M.; Dodelet, J.-P.; Kramm, U. I.; Herrmann, I.; Bogdanoff, P.; Maruyama, J.; Nagaoka, T.; Garsuch, A.; Dahn, J. R.; Olson, T.; Pylypenko, S.; Atanassov, P.; Ustinov, E. A. *ACS Appl. Mater. Interfaces* **2009**, *1*, 1623.

(18) Lefevre, M.; Proietti, E.; Jaouen, F.; Dodelet, J.-P. *Science (Washington, DC, U. S.)* **2009**, *324*, 71.

(19) Proietti, E.; Jaouen, F.; Lefevre, M.; Larouche, N.; Tian, J.; Herranz, J.; Dodelet, J.-P. *Nat. Commun.* **2011**, *2*, 416.

(20) Wu, G.; More, K. L.; Johnston, C. M.; Zelenay, P. *Science (Washington, DC, U. S.)* **2011**, *332*, 443.

(21) Zagal, J. H. In *N4-Macrocyclic Metal Complexes*; Zagal, J. H., Bedioui, F., Dodelet, J.-P., Eds.; Springer: New York, 2006; p 41.

(22) Oyaizu, K.; Murata, H.; Yuasa, M. Macrocyles for Fuel Cell Cathodes. In *Molecular Catalysts for Energy Conversion*; Okada, T., Kaneko, M., Eds.; Springer Series in Materials Science; Springer: Berlin Heidelberg: 2009; Vol. *111*, p 139.

(23) Xu, Y.; Shao, M.; Mavrikakis, M.; Adzic, R. R. In *Fuel Cell Catalysis: A Surface Science Approach*; Koper, M. T. M., Ed.; John Wiley & Sons, Inc.: Hoboken, NJ, 2009.

(24) Reed, C. A.; Cheung, S. K. *Proc. Natl. Acad. Sci. U. S. A.* **1977**, *74*, 1780.

(25) Nakashima, H.; Hasegawa, J.-Y.; Nakatsuji, H. *J. Comput. Chem.* **2006**, *27*, 426.

(26) Zagal, J. H.; Gulppi, M.; Isaacs, M.; Cardenas-Jiron, G.; Aguirre, M. J. *Electrochim. Acta* **1998**, *44*, 1349.

(27) Beck, F. *J. Appl. Electrochem.* **1977**, *7*, 239.

(28) Liao, M.-S.; Scheiner, S. *J. Chem. Phys.* **2002**, *117*, 205.

(29) Kadish, K. M.; Van Caemelbecke, E.; Royal, G. In *Porphyrin Handbook*; Kadish, K. M., Smith, K. M., Guilard, R., Eds.; Academic Press: San Diego, CA, 2000; Vol. *8*, p 1.

(30) Yamashige, H.; Matsuo, S.; Kurisaki, T.; Perera, R. C. C.; Wakita, H. *Anal. Sci.* **2005**, *21*, 309.

(31) Yamazaki, S.; Yamada, Y.; Ioroi, T.; Fujiwara, N.; Siroma, Z.; Yasuda, K.; Miyazaki, Y. *J. Electroanal. Chem.* **2005**, *576*, 253.

(32) Ljubisa, R. In *Carbons for Electrochemical Energy Storage and Conversion Systems*; CRC Press: Boca Raton, FL, 2009; p 163.

(33) Burg, P.; Cagniant, D. In *Chemistry & Physics of Carbon*; Radovic, L. R., Ed.; CRC Press: Boca Raton, FL, 2007; p 129.

(34) Darmstadt, H.; Roy, C. *Carbon* **2003**, *41*, 2662.

(35) Bard, A. J. *J. Am. Chem. Soc.* **2010**, *132*, 7559.

(36) Ramaswamy, N.; Mukerjee, S. *J. Phys. Chem. C* **2011**, *115*, 18015.
(37) Ramaswamy, N.; Allen, R. J.; Mukerjee, S. *J. Phys. Chem. C* **2011**, *115*, 12650.
(38) Markovic, N.; Gasteiger, H.; Ross, P. N. *J. Electrochem. Soc.* **1997**, *144*, 1591.
(39) Murthi, V. S.; Urian, R. C.; Mukerjee, S. *J. Phys. Chem. B* **2004**, *108*, 11011.
(40) Teliska, M.; O'Grady, W. E.; Ramaker, D. E. *J. Phys. Chem. B* **2005**, *109*, 8076.
(41) Mukerjee, S.; Arruda, T. *Mod. Aspects Electrochem.* **2010**, *50*, 503.
(42) Bae, I. T.; Tryk, D. A.; Scherson, D. A. *J. Phys. Chem. B* **1998**, *102*, 4114.
(43) Ankudinov, A. L.; Ravel, B.; Rehr, J. J.; Conradson, S. D. *Phys. Rev. B: Condens. Matter Mater. Phys.* **1998**, *58*, 7565.
(44) Bouwkamp-Wijnoltz, A. L.; Visscher, W.; van Veen, J. A. R.; Boellaard, E.; van der Kraan, A. M.; Tang, S. C. *J. Phys. Chem. B* **2002**, *106*, 12993.
(45) Tanaka, A.; Gupta, S. L.; Tryk, D.; Fierro, C.; Yeager, E. B.; Scherson, D. A. *Proc. - Electrochem. Soc.* **1992**, *92-11*, 555.
(46) Pacilé, D.; Papagno, M.; Rodríguez, A. F.; Grioni, M.; Papagno, L.; Girit, Ç. Ö.; Meyer, J. C.; Begtrup, G. E.; Zettl, A. *Phys. Rev. Lett.* **2008**, *101*, No. 066806.
(47) Ramm, M.; Ata, M.; Brzezinka, K.-W.; Gross, T.; Unger, W. *Thin Solid Films* **1999**, *354*, 106.
(48) Maldonado, S.; Morin, S.; Stevenson, K. J. *Carbon* **2006**, *44*, 1429.
(49) Takahagi, T.; Ishitani, A. *Carbon* **1988**, *26*, 389.
(50) Zagal, J. H.; Cardenas-Jiron, G. I. *J. Electroanal. Chem.* **2000**, *489*, 96.
(51) Cardenas-Jiron, G. I.; Gulppi, M. A.; Caro, C. A.; del Rio, R.; Paez, M.; Zagal, J. H. *Electrochim. Acta* **2001**, *46*, 3227.
(52) Shigehara, K.; Anson, F. C. *J. Phys. Chem.* **1982**, *86*, 2776.